ISSN 1066-3622, Radiochemistry, 2019, Vol. 61, No. 3, pp. 339–346. © Pleiades Publishing, Inc., 2019.
Russian Text © The Authors, 2019, published in Radiokhimiya, 2019, Vol. 61, No. 3, pp. 244–250.

Dynamics of Sorption–Desorption of ^{223}Ra Therapeutic α-Emitter on Granulated Hydroxyapatite

A. V. Severin*[a], A. N. Vasil'ev[a,b], A. V. Gopin[a], I. E. Vlasova[a], and E. V. Chernykh[a]

[a] *Chemical Department, Moscow State University, Moscow, 119991 Russia*
[b] *Institute for Nuclear Research, Russian Academy of Sciences, ul. Fizicheskaya 27, Troitsk, Moscow, 108840 Russia*
**e-mail: severin@radio.chem.msu.ru*

Received June 06, 2018; revised November 26, 2018; accepted November 27, 2018

Abstract—The dynamics of the ^{223}Ra distribution in the volume of spherical hydroxyapatite (HAP) granules in the course of the ^{223}Ra sorption from aqueous solutions onto sorbent particles and desorption was studied by α-track radiography. The optimum time of contact of the sample with a detector (exposure) was found, and a procedure for preparing experimental samples was suggested. Taking into account the density of the porous sorbent, the ranges of the α-particles emitted by ^{223}Ra and its daughter products and of the recoil nuclei were estimated. The averaged effective range of the α-particles in HAP is ~35 μm. A mathematical model of the Ra diffusion into the depth of the porous sorbent, taking into account the sorption, was developed on the basis of the parameters obtained. The effective diffusion coefficient was estimated at ~3×10^{-5} cm^2 s^{-1}. Correlation between the sorbent particle size, radionuclide sorption time, and the absorbed dose produced by the particle in a biological tissue was demonstrated.

Keywords: nuclear medicine, radium, hydroxyapatite, α-track radiography

DOI: 10.1134/S1066362219030093

The progress of nuclear medicine is associated both with the development of novel radiopharmaceuticals (RPs) based on promising diagnostic and therapeutic radionuclides and with the improvement of methods for the RP delivery and functioning in a living body. The RP development requires appropriate (from the viewpoint of nuclear-physical and chemical characteristics) α- and β-emitters, and also their carriers. Inorganic nano- and microparticles are suggested as carriers more and more frequently [1]. Among such particles, hydroxyapatite (HAP, inorganic matrix of bone tissues) is one of the most promising, because it is biocompatible, bioresorbable, and often bioactive. It is successfully used in medical practice for a long time [2]; in particular, it is suggested as radionuclide carrier for nuclear medicine [3–5]. HAP is often used as a model system for studying RPs for diagnostics or therapy of skeleton diseases, and also in radiosynovectomy, a method for treating chronic inflammation diseases of joints, when radioactive sols and suspensions are injected directly into the joint. A promising therapeutic α-emitter is ^{223}Ra; Xofigo® preparation (Bayer) based on it is used for therapy of tumor diseases [6, 7]. This is the first and, by now, the only RP based on an α-emitter, approved by the US Food and Drug Administration (USFDA). Xofigo is an $RaCl_2$ solution; its action is based on the similarity of the biochemical behavior of the Ca and Ra ions, and the application field is limited to bone metastases of various types of cancer.

Alternative procedures for the radionuclide delivery and retention in the site of therapy are also being searched for. These include radium incorporation into liposomes [8, 9] and into nano- and microparticles of nanozeolites [10, 11], lanthanum phosphate [12], and calcium carbonate [13].

The idea of combining Ra and hydroxyapatite is not novel [14–16]. The relationships of the Ra sorption onto HAP were studied in [15, 16], and attempts were made to introduce ^{223}Ra in the course of the HAP synthesis. In [16], we determined the optimum conditions for spiking with 98% yield: solid-to-liquid ratio, contact time, pH of solution. As a result of annealing of the spiked HAP particles, the ^{223}Ra washout in vitro does not exceed 5%. When developing an RP, it is important not only to know the integral values of the ra-

dionuclide sorption onto and desorption from the carrier, but also to study in detail the Ra distribution in the volume of the porous support in the course of sorption and desorption. This is necessary for calculating the dose absorbed by the body and, correspondingly, the required activity of the radionuclide administered for therapeutic purposes. One of the most informative methods for solving this problem is α-track radiography.

α-Track radiography is based on the ability of dielectrics to record tracks of charged particles, including α-particles, with spatial resolution [17]. α-Track radiography allows determination of the number of α-particles emitted by the source being analyzed into the track detector plane and of the α-particle track direction and estimation of the α-particle energy [18]. Polycarbonate α-track detectors of CR-39 type, exhibiting the best characteristics from the viewpoint of spatial and energy resolution [19, 20], give the most informative images of α-particle tracks. Previously we demonstrated the possibility of applying this method to HAP-^{223}Ra samples [16].

Thus, this study was aimed at imaging the dynamics of the ^{223}Ra penetration into the depth of porous HAP granules and of its redistribution in sorption–desorption processes, and also at estimating the effective diffusion coefficient of ^{223}Ra and its decay products and the range of α-particles formed in the ^{223}Ra decay chain in various materials for the subsequent calculation of the absorbed dose rate around the HAP nanoparticle.

EXPERIMENTAL

^{223}Ra was produced by irradiating a natural Th target with medium-energy protons (120–90 MeV) at the Institute for Nuclear Research, Russian Academy of Sciences (Troitsk, Moscow, Russia) and was isolated and purified as a hydrochloric acid solution in accordance with the published procedure [21]. Directly before the sorption experiment, the solution was neutralized with 0.1 M NaOH to pH ~ 5–7.

The activity of solution samples was measured with a γ-ray spectrometer equipped with a GR3818 high-purity germanium semiconductor γ-ray detector (Canberra, the United States). The γ-ray spectra were processed using Genie 2000 software (Canberra). The ^{223}Ra activity was calculated using the 154 keV peak [22].

HAP nanoparticles were prepared by the procedure described in [23]. In a typical experiment, a 3.1 M H_3PO_4 solution was introduced at a controllable rate to pH 6.5–7.0 into a temperature-controlled reactor (298 K) filled with a stirred 16 mg mL^{-1} $Ca(OH)_2$ suspension. The reactant concentrations were chosen so as to obtain a 5% suspension of the product. After adding the whole amount of the acid, the mixture was stirred for 2 h.

Granulated hydroxyapatite was prepared by mechanically stimulated morphological selection in the course of boiling the HAP suspension in accordance with the procedure described in detail elsewhere [24]. The morphology of the spherical HAP particles obtained was characterized by scanning electron microscopy (SEM, CamScan device, Japan, resolution 5 nm). The free specific surface area of the dry samples was determined by mercury porosimetry with a Porosimeter 2000 device (Germany).

The optimum conditions for performing the sorption experiments (pH, ratio of the sorbent weight and solution volume) were preliminarily determined in our previous study [16]. The sorbent samples were prepared by preliminary selection of spherical HAP samples of similar size (sphere diameter 900–1000 μm). The sorbent weighed portion (~10 mg, or 19 spherical granules) was placed in a 1.5-mL Eppendorf plastic test tube, after which the sorbent was wetted with distilled water and stirred for 24 h to remove air from the internal free volume of the pores. After that, a 1-mL portion of the Ra solution with the activity concentration of 10 kBq mL^{-1} (100 μL of $^{223}RaCl_2$ solution and 900 μL of H_2O) was added into each test tube. The test tubes were shaken for the required time with a REAXtop vortex (Heidolf, Germany). The sorption time was 1, 5, 15, 30, 60, 180, and 1440 min. Then, the phases were separated by centrifugation (Allegra 64R centrifuge, Beckman Coulter, the United States), and a 0.75-mL portion of the solution was measured on a γ-ray spectrometer. The radionuclide fraction taken up by the solid phase was calculated from the difference between the activity concentrations of the initial and final solutions, and the sorption kinetic curve was plotted. The remaining granules were separated from the sorbate solution, washed 2 times with ethanol, and dried in an Eppendorf test tube or on a filter paper in air. After that, the granules (ten spherical particles per time point) were cut into halves with a special microtome, and the halves were placed on a flat

support onto double-sided scotch tape in different fashions: the section surface or the round surface of the granule upwards.

Track radiography was performed with a CR-39 detector [special poly(allyl diglycol carbonate) support, TASTRAK®, the United Kingdom]. The detector was put on the samples from above and kept for the empirically chosen exposure time. Then, the detector was washed with distilled water and etched in a 6.25 M NaOH solution for 4 h at 80°C, after which it was again washed with distilled water and dried in air. The images of pits from etching α-particle tracks were taken with an Olympus BX-51 optical microscope equipped with an E-330 digital camera. The images obtained were analyzed using ImageScope M program. When counting the number of decays at a definite distance from the granule center, we took into account only the tracks directed perpendicular to the detector plate plane (they form regular circles in the projection onto the detector plane).

The Ra desorption experiments were performed similarly. Each Eppendorf tube was charged with 19 HAP spheres (10 mg), 150 μL of a $^{223}RaCl_2$ solution, and 850 μL of H_2O; the sorption was performed for 24 h. After that, we removed the solution and leached Ra with 1 mL of a 0.9% NaCl solution. Further procedure was similar to that used for the above-described sorption experiments.

All the experiments were performed at 22 ± 2°C.

RESULTS AND DISCUSSION

The HAP granules used in the study were spherical particles with relatively dense and uniform internal structure (Fig. 1). Particles 900–1000 μm in diameter were used; this size seemed to be optimum for autoradiographic imaging of the radium sorption. According to the data of mercury porosimetry, the particles had the free specific surface area of 72 $m^2\ g^{-1}$ and the porosity of approximately 60%.

The ^{223}Ra sorption kinetics is shown in Fig. 2. The sorption equilibrium in the system is attained in 60–80 min.

The results of the track radiography of the HAP samples after the ^{223}Ra sorption were analyzed at different detector exposure times, 1 and 24 h. At the exposure time of 24 h, the track density appeared to be too high, and many tracks overlapped. This fact strongly complicates their subsequent counting. Therefore, we chose the exposure time of 1 h, which ensures the maximum possible number of discernible individual tracks.

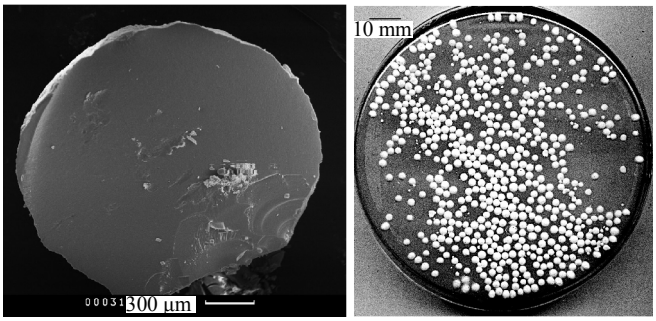

Fig. 1. Images of HAP granules, taken with (a) SEM and (b) optical microscope.

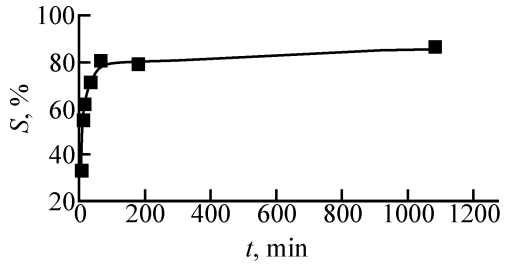

Fig. 2. Kinetics of ^{223}Ra sorption onto spherical HAP. m(HAP) = 10 mg, d = 0.5–2.0 mm, 1 mL of solution, pH 6–7.

The positions and number of α-tracks on the granule sections significantly changed depending on the sorption time. The tracks were redistributed from the particle periphery to its center (Fig. 3). The desorption data (approximately 20% of the introduced activity was desorbed) show that the process occurs uniformly throughout the depth of the HAP granule.

Our main goals, along with testing the autoradiographic procedure, were determinatoin of the range of the ^{223}Ra α-particles in the sorbent material and estimation of the effective coefficient of the diffusion of Ra and its decay products into the depth of the porous HAP granule. In addition, we estimated the influence of the HAP spiking time on the effective absorbed dose produced by the sample.

To determine the influence of the ^{223}Ra distribution in HAP microspheres on the produced dose, it is necessary to calculate the range of α-particles in hydroxyapatite. HAP at the stoichiometric composition $Ca_{10}(PO_4)_6(OH)_2{\cdot}3H_2O$ has the crystallographic density of 3.14 g cm^{-3}; the HAP spheres exhibit 60% po-

Table 1. Mean energy and range of α-particles emitted by ^{223}Ra and its decay products in water, biological tissue, and hydroxyapatite [$R_{HAP(900)}$, range of α-particles in hydroxyapatite spheroids annealed for 3 h at 900°C in a muffle furnace; E_α^m, weighted mean α-particle energy)

Nuclide	$T_{1/2}$	E_α^m, keV	R_{aq}	R_{bio}	R_{HAP}	$R_{HAP(900)}$
			μm			
^{223}Ra	11.43 days	5644.6	41	55	28	21
^{219}Rn	3.96 s	6748.7	54	72	37	27
^{215}Po	1.78 ms	7385.4	61	82	42	31
^{211}Bi	2.14 min	6549.2	51	69	35	26
^{211}Po	0.52 s	7442.4	62	83	42	31
Mean		6583	52	69	35	26
σ		719	8	11	6	4

rosity. As a result of annealing at 900°C, the porosity decreases to 15%, and the sample loses water of crystallization. We believe that the pores are distributed uniformly throughout the granule volume and are filled with water. Then, to determine the range of α-particles, we used the formulas [25]

$$1/R_{HAP+aq} = 1/R_{HAP} + 1/R_{aq}, \quad (1)$$

$$1/R_{HAP} = \omega_{Ca}/R_{Ca} + \omega_O/R_O + \omega_P/R_P + \omega_H/R_H, \quad (2)$$

$$1/R_{aq} = \omega_O/R_O + \omega_H/R_H, \quad (3)$$

$$R_z = R_{air}[(0.90 + 0.0275Z) + (0.06 - 0.086Z)\ln(E/4)], \quad (4)$$

$$R_{air} = 0.381E^{3/2}[-b \pm (b^2 - 4ac)^{1/2}]/(2a), \quad (5)$$

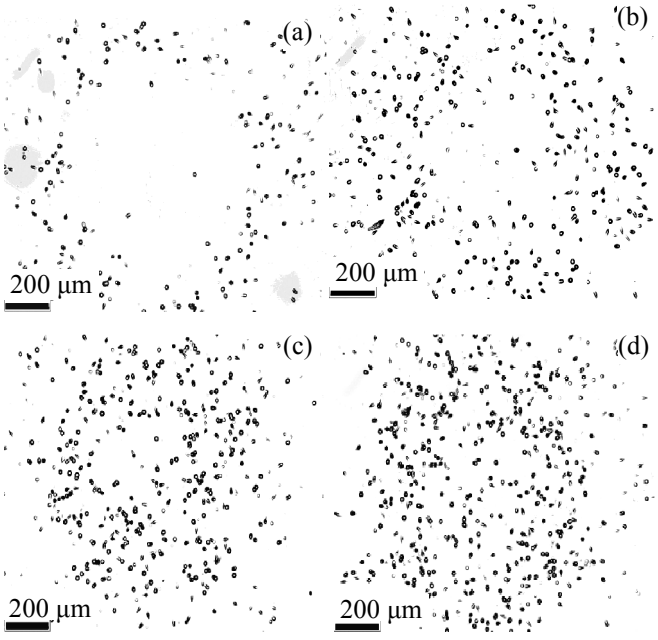

Fig. 3. α-Track images of the cross section of HAP granules after ^{223}Ra diffusion into the depth of the granules. Sorption time: (a) 5 min, (b) 30 min, (c) 3 h, and (d) 24 h. Exposure time of α-track detector on HAP granules 1 h.

where R_z is the range of α-particles (mg cm^{-2}) in a medium (in separate elements or in a complex substance; HAP denotes hydroxyapatite; aq, water; HAP+aq, HAP with pores filled with water); ω_z, relative content of element z in the mixture or compound; E, α-particle energy (MeV); Z, atomic number of element z contained in the substance. For hydrogen, the sum 0.90 + 0.0275Z in (4) is replaced by 0.3. The results of calculating the range of α-particles emitted by ^{223}Ra and its decay products are given in Table 1 (we used in the calculations the energies of all the α-particles of the parent and daughter radionuclides and their yields per decay, taken from [22]).

To determine the range in a uniform medium (biological tissue), we used the formula

$$R_{bio} = AE^{3/2}/(\rho Z^{2/3}), \quad (6)$$

where A is the mean atomic mass of the medium (15.7); ρ, density of the medium (1 g cm^{-3}); and R_{bio}, range (μm). The maximal range of α-particles was R = 83 μm (for ^{211}Po, E_α = 7.44 MeV) (Table 1). For hydroxyapatite, the mean range was 35 μm, and after the annealing it decreased to 26 μm.

As a result of successive chain of α-decays, ^{223}Ra emits four α-particles with the mean energy of 6.6 MeV (Table 1). In each decay event, the daughter nuclei acquire the recoil kinetic energy of ~100–145 keV. In the case of the production of ^{211}Bi and ^{211}Pb, the hot atoms abstracted from the crystal structure after the exhaustion of the energy that they acquired can be sorbed by the carrier with high probability [26, 27]. Another daughter radionuclide, ^{219}Rn, combines chemical inertness with short half-life (about 4 s), sufficient, however, for a significant part of ^{219}Rn to migrate from the therapy site. Using SRIM-2013

software [28], we calculated the range of ^{219}Rn recoil nuclei (E = 103.1 keV) in various materials (Table 2).

Along with spherical particles 900–1000 μm in diameter, chosen for the study, it seems also necessary to consider spiking of HAP nanoparticles, when the RP is a radioactive suspension. Taking into account the characteristics of HAP nanoparticles (length up to 500, width up to 100, thickness up to 0.8–2.4 nm [29]), we can conclude that, when using them as a ^{223}Ra carrier, up to 100% of the ^{219}Rn recoil nuclei will be ejected beyond the HAP nanoplates. Thus, from the viewpoint of nuclear-physical characteristics of ^{223}Ra and its decay products, the best carriers are HAP spheroids capable to retain inside the particle the hot atoms produced by the decay.

The performance of HAP spheroids as α-emitter carriers will depend on the radionuclide distribution inside the particle, because a part of α-particles will be absorbed within the carrier. To simulate such distribution, it is necessary to estimate, along with the quantitative characteristics of sorption–desorption, also the effective diffusion of Ra and its decay products inside the particle.

The ^{223}Ra distribution was analyzed as follows: The cross section of a spherical granule (r = 450–550 μm) was divided into circular sectors 100 μm thick, and the number of perpendicular tracks in each sector was calculated (Fig. 4). Assuming that, by so doing, we visualize the tracks from α-particles that were emitted by Ra and its decay products and reached the surface of the HAP particles from the depth of no more than 35 μm, we can pass to the number of tracks in the selected volume of a spherical particle and thus to the total number of tracks in the given granule at each moment of sorption. Knowing the sorption kinetics, we can relate the number of tracks in a particle to the real absolute activity and activity concentration of ^{223}Ra. The roughest estimation of the diffusion coefficient from the time of filling of the granule center (30 min, Fig. 3b) gives the value of the order of 10^{-6} cm^2 s^{-1}. For the more rigorous calculation, we used the approach described below.

Because analytical estimation of the diffusion parameters of an active component in the radial symmetry is rather difficult, we attempted to create a model of its distribution inside the sorbent granule. The model takes into account the supply of the active component from the external solution into the sorbent granule and its diffusion and sorption in the granule.

Table 2. Range of ^{219}Rn recoil nuclei (E = 103.1 keV) in various materials

Material	Density, g cm^{-3}	Range, nm
Water	1.00	84
HAP (without pores)	3.14	33
HAP (60% pores filled with water)	1.86	52
HAP (900) (15% pores filled with water)	2.82	37
Cortical bone	1.92	49

For a spherical granule, in the case of radial symmetry, the equation for the transfer of the active component can be written as follows:

$$\partial C/\partial t = D(\partial^2 C/\partial r^2 + 2r^{-1}\partial C/\partial r) - q. \quad (7)$$

Here, $C(r,t)$ is the component concentration profile; q, function taking into account the component consumption in sorption. In this case, we made an assumption that this function is independent of r and t and linearly depends on C, with the consumption ceasing when the limiting sorption is reached. Thus, the expression for q will be as follows:

$$q(C,r,t) = \begin{cases} kC(r,t) \text{ at } \Gamma(r,t) < \Gamma_{max} \\ 0 \text{ at } \Gamma(r,t) = \Gamma_{max}. \end{cases} \quad (8)$$

Here, $\Gamma(r,t)$ is the sorption profile of the active component, and Γ_{max} is its limiting sorptions.

In the initial time moment, the granule contained nether dissolved nor sorbed component:

$$C(r,0) = 0, \ 0 < r < R, \quad (9)$$

$$\Gamma(r,0) = 0, \ 0 < r < R, \quad (10)$$

where R is the granule radius.

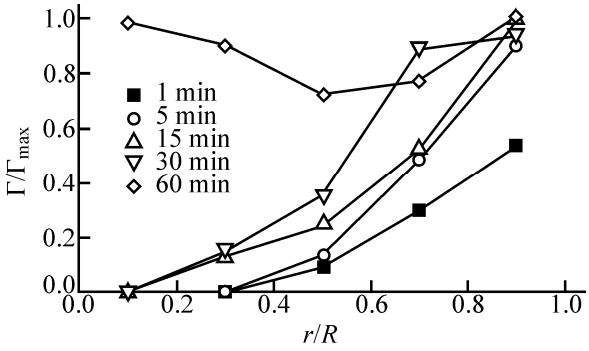

Fig. 4. Experimental sorption profiles of the active component.

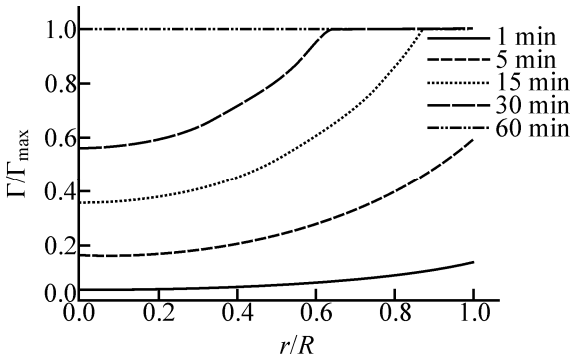

Fig. 5. Sorption profiles of the active component at k = 0.2 Bq cm^{-3} s^{-1} and $D = 5 \times 10^{-5}$ cm^2 s^{-1}.

The boundary condition at $r \to 0$ can be written as follows:

$$\partial C/\partial t = 3\partial^2 C/\partial r^2. \quad (11)$$

The concentration at the granule boundary is determined by the concentration of the active component in the external solution C_M:

$$C(R,t) = C_M(t). \quad (12)$$

It decreases with the progress of sorption inside the granule:

$$C_M(t) = [\nu_0 - \nu_C(t) - \nu_\Gamma(t)]/V_M. \quad (13)$$

Here, ν_0 is the initial amount of the active component in the external solution, ν_C and ν_Γ are its amounts in the solution and in the sorbed form inside the granule, and V_M is the external solution volume.

Problem (7) with initial and boundary conditions (9)–(12) and dependences (8) and (13) is a nonlinear nonstationary problem. Its solution was found by numerical methods in the simplest unidimensional case. To this end, we replaced the derivatives by finite differences using the Crank–Nicolson method and solved the linear equation system obtained by the tridiagonal matrix algorithm. We performed in this study of series of computational experiments with different sets of parameters determining the diffusion and sorption rates.

As seen from the experimental data, the central part of the granule becomes completely filled in 60 min (Fig. 4). On the other hand, in a shorter time the active component does not noticeably penetrate there. Therefore, it can be assumed that the diffusion is the limiting factor in this case. This assumption is confirmed by the

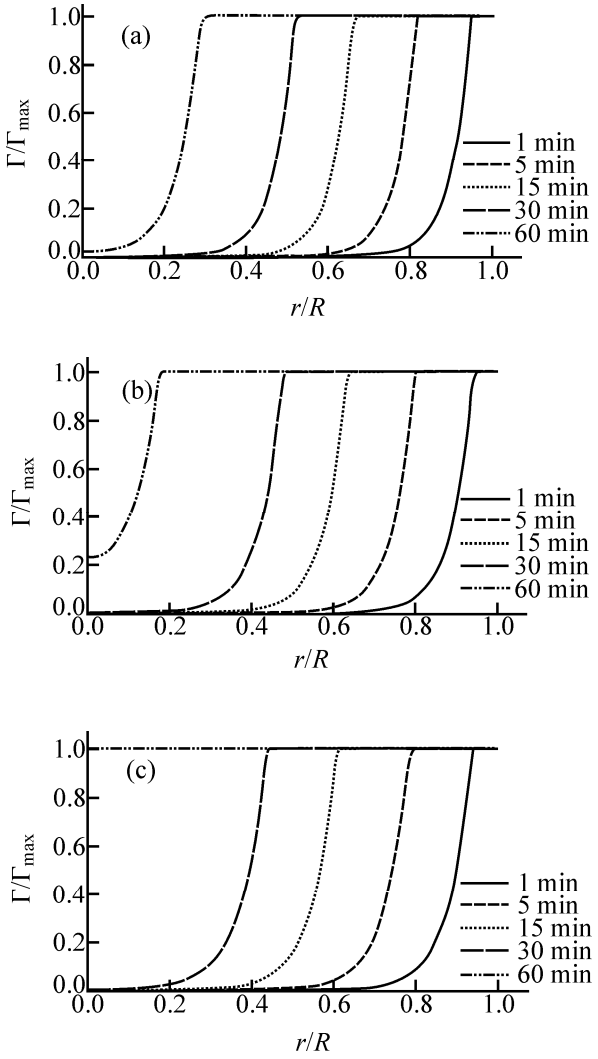

Fig. 6. Sorption profiles of the active component at k = 5 Bq cm^{-3} s^{-1} and D = (a) 2.5×10^{-5}, (b) 3×10^{-5}, and (c) 3.5×10^{-5} cm^2 s^{-1}.

results of the computational experiment. Figure 5 shows the sorption profiles of the active component at k = 0.2 Bq cm^{-3} s^{-1} and $D = 5 \times 10^{-5}$ cm^2 s^{-1}. In this case, the limiting factor is sorption. This leads to the situation when the active component rapidly penetrates into the whole volume of the granule, and only after that its sorption increases.

Figure 6 shows the sorption profiles of the active component at k = 5 Bq cm^{-3} s^{-1} and $D = 2.5 \times 10^{-5}$, 3×10^{-5}, and 3.5×10^{-5} cm^2 s^{-1}. Specifically the sorbed fraction mainly determines the granule radioactivity, which follows from the ratios of the external solution and granule volumes and of their activities after the sorption. As can be seen, as the diffusion coefficient is

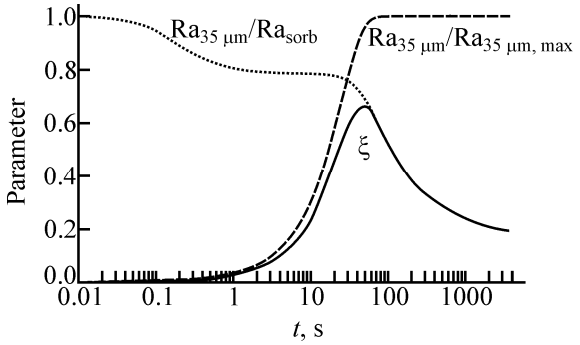

Fig. 7. Parameters of the diffusion and sorption components of the absorbed dose produced in the tissue surrounding the granule and product of these parameters (ξ) as functions of the sorption time.

increased from 2.5×10^{-5} to 3.5×10^{-5} cm^2 s^{-1}, filling of the central part of the granule changes ($r/R < 0.2$). For example, at $D = 2.5 \times 10^{-5}$ cm^2 s^{-1} the central part contains virtually no active component (Fig. 6a), at $D = 3 \times 10^{-5}$ cm^2 s^{-1} it is filled partially (Fig. 6b), and at $D = 3.5 \times 10^{-5}$ cm^2 s^{-1} it is completely filled with the sorbed active component (Fig. 6c). The latter case is actually observed in the experiment. It should be noted, however, that the experimental sorption profiles differ significantly from those obtained using the above-described model. This may be due to the complex internal texture of the granule and to the deviation of its shape from a sphere, which leads to significant deviation of the solution from that obtained in this study.

Thus, it can be assumed that filling of the granule with the active component is diffusion-controlled. The diffusion coefficient is ~3×10^{-5} cm^2 s^{-1}.

With the numerical expression for the sorption, the size of HAP particles, the range of α-particles in them, and their distribution in the spherical particles known, we can estimate the absorbed dose produced by the given radionuclide in a living body (tumor cells). To reach the maximal absorbed dose, it is necessary to vary the particle size and the sorption time.

To a first approximation, the absorbed dose in the tissue surrounding a granule is proportional to the radionuclide fraction in the external surface of the granule ($Ra_{35\ \mu m}$), whose thickness does not exceed the α-particle range, relative to the activity in the whole granule (Ra_{sorb}) (curve $Ra_{35\ \mu m}/Ra_{sorb}$, Fig. 7). Apparently, at the beginning of the sorption this fraction is equal to 1; then, with the progress of radium diffusion in a granule, it tends to an equilibrium value (diffusion component). On the other hand, the absorbed dose is proportional to the ratio of the activity in the external layer to the maximum activity in the external layer that can be reached under the given sorption conditions (curve $Ra_{35\ \mu m}/Ra_{35\ \mu m,\ max}$, Fig. 7). Under the conditions of constant activity concentration of Ra in the solution, this ratio tends to 1 (sorption component). The product of the diffusion and sorption components allows determination of the spiking parameters ensuring the formation of the most effective product from the viewpoint of the transfer of the radiation energy to the tissue (curve ξ in Fig. 7).

The obtained dependence of ξ can be accounted for as follows: First, the majority of Ra ions are on the HAP surface, but the sorption is very low (less than 10%). Then, the radionuclide sorption and the absorbed dose produced by it in the surrounding tissue increase in the parallel fashion, but by the time t_s = 1 min the dose transferred to the surrounding tissue decreases, because a fraction of Ra migrates inside the sorbent particle, and its α-particles become absorbed by the granule material (or lose the major fraction of their energy) and become incapable of killing tumor cells.

Thus, the ^{223}Ra distribution in hydroxyapatite spheroids in relation to the sorption time was imaged using track autoradiography. The dependences obtained were analyzed, and the effective diffusion coefficient, ~3×10^{-5} cm^2 s^{-1}, was calculated. The ranges of α-particles and ^{219}Rn recoil nuclei in the carrier material were calculated, and the optimum sorption time (1 min) at which the largest fraction of α-particles from the RP obtained reaches the tumor cells was estimated from these data.

FUNDING

The study was financially supported by the Russian Foundation for Basic Research (projects 16-33-00200 and 18-03-00432). The use of the equipment of the Center for Shared Use, Institute for Nuclear Research, Russian Academy of Sciences was supported by Agreement no. 14.621.21.0014 with the Ministry of Education and Science of the Russian Federation (unique project identifier RFMEF162 117X0014).

CONFLICT OF INTEREST

The authors declare that they have no conflict of interest.

REFERENCES

1. Hamoudeh, M., Kamleh, M.A., Diab, R., and Fessi, H., *Adv. Drug Deliv. Rev*., 2008, vol. 60, no. 12, pp. 1329–1346.
2. Bohner, M., *Injury*, 2000, vol. 31, pp. 37–47.
3. Chakraborty, S., Das, T., Sarma, H.D., et al., *Nucl. Med. Biol*., 2008, vol. 35, pp. 589–597.
4. Albernaz, M.D.S., Ospina, C.A., Rossi, A.M., and Santos-Oliveira, R., *Art. Cells Nanomed. Biotechnol*., 2014, vol. 42, no. 2, pp. 88–91.
5. Kothari, K., Suresh, S., Sarma, H.D., et al., *Appl. Radiat. Isot*., 2003, vol. 58, no. 4, pp. 463–468.
6. Trewartha, D. and Carter, K., *Nat. Rev. Drug Discov*., 2013, vol. 12, pp. 823–824.
7. Den, R.B., Doyle, L.A., and Knudsen, K.E., *Can. J. Urol*., 2014, vol. 21, suppl. 1, pp. 70–76.
8. Henriksen, G., Schoultz, B.W., Michaelsen, T.E., et al., *Nucl. Med. Biol*., 2004, vol. 31, pp. 441–449.
9. Jonasdottir, T.J., Fisher, D.R., Borrebaek, J., et al., *Anticancer Res*., 2006, vol. 26, pp. 2841–2848.
10. Piotrowska, A., Leszczuk, E., Bruchertseifer, F., et al., *J. Nanopart. Res*., 2013, vol. 15, p. 2082.
11. Piotrowska, A., Meczynska-Wielgosz, S., Majkowska-Pilip, A., et al., *Nucl. Med. Biol*., 2017, vol. 47, pp. 10–18.
12. Rojas, J.V., Woodward, J.D., Chen, N., et al., *Nucl. Med. Biol*., 2015, vol. 42, pp. 614–620.
13. Westrøm, S., Malenge, M., Jorstad, I.S., et al., *J. Label. Compd. Radiopharm*., 2018, vol. 61, pp. 472–486.
14. Larsen, R.H. and Salberg, G., Patent US 8 142 758, 2012.
15. Kozempel, J., Vlk, M., Malkova, E., et al., *J. Radioanal. Nucl. Chem*., 2015, vol. 304, pp. 443–447.
16. Vasiliev, A.N., Severin, A., Lapshina, E., et al., *J. Radioanal. Nucl. Chem*., 2017, vol. 311, no. 2, pp. 1503–1509.]
17. Fleischer, R.L., Price, P.B., and Walker, R.M., *Nuclear Tracks in Solids: Principles and Applications*, Univ. of California Press, 1975.
18. Ilić, R. and Durrani, S.A., *Handbook of Radioactivity Analysis*, L'Annunziata, M., Ed., Academic, 2003, 2nd ed., pp. 179–237.
19. Dorschel, B., Hermsdorf, D., Reichelt, U., et al., *Radiat. Meas*., 2003, vol. 37, pp. 563–571.
20. Fromm, M., Membrey, F., El Rahmany, A., and Chambaude, A., *Nucl. Tracks Radiat. Meas*., 1993, vol. 21, pp. 357–365.
21. Vasiliev, A.N., Ostapenko, V.S., Lapshina, E.V., et al., *Radiochim. Acta*, 2016, vol. 104, no. 8, pp. 539–547.
22. National Nuclear Data Center, Brookhaven National Laboratory (USA), http://www.nndc.bnl.gov/nudat2.
23. Melikhov, I.V., Komarov, V.F., Severin, A.V., et al., *Dokl. Phys. Chem*., 2000, vol. 373, pp. 125–128.
24. Severin, A.V., Komarov, V.F., Bozhevol'nov, V.E., and Melikhov, I.V., *Russ. J. Inorg. Chem.*, 2005, vol. 50, no. 1, pp. 72–77.
25. Nemets, O.F. and Gofman, Yu.F., *Spravochnik po yadernoi fizike* (Handbook of Nuclear Physics), Kiev: Naukova Dumka, 1975.
26. Akkaya, R., *J. Radioanal. Nucl. Chem*., 2012, vol. 292, no. 2, pp. 771–775.
27. Morsy, R., *Arab. J. Sci. Eng*., 2016, vol. 41, no. 6, pp. 2185–2191.
28. Ziegler, J.F., *SRIM-2013 Code*, http://www.srim.org.
29. Suvorova, E.I., Klechkovskaya, V.V., Komarov, V.F., et al., *Crystallogr. Rep*., 2006, vol. 51, no. 5, pp. 881–887.

Translated by G. Sidorenko